Journal of Structural Geology, Vol. 1, No. 4, 1979, pp. 317 to 321.
Pergamon Press Ltd. 1980. Printed in Great Britain.

The representation and calculation of the deviatoric component of the geological stress tensor

RICHARD J. LISLE*

Geologisch Instituut, Rijksuniversiteit Leiden, The Netherlands

(*Received* 21 *August* 1979; *accepted in revised form* 9 *November* 1979)

Abstract—A new diagram for the representation of stress states is proposed and compared with Nadai's stress diagram. The diagram is a graph whose axes are labelled as the differences of the principal stresses ($\sigma_2 - \sigma_3$ as ordinate axis, $\sigma_1 - \sigma_2$ as the abscissa; where $\sigma_1 > \sigma_2 > \sigma_3$ are the principal stresses). The design of the plot has been deliberately modelled on that of the 'log Flinn' diagram which is used to represent finite strain ellipsoids. The position of the plotted stress state on this diagram depends on the nature of the deviatoric (non-hydrostatic) component of the stress tensor. The distance of the plotted stress from the origin corresponds broadly to the departure of the stress from a hydrostatic state and the parameter R, defined as the gradient of the line joining the plotted state to the origin, expresses the type of symmetry possessed by the stress tensor.

It is explained how the diagram can be used to represent calculated palaeostresses and, in particular, how the parameter R can be found directly from some existing methods of stress analysis currently in use.

Besides its proposed function to represent the results of such analyses it is felt that the use of the diagram may make clear the essential elements of the definitions of well-known terms used to describe particular stress states (e.g. plane stress, triaxial stress, axial compression, etc.).

INTRODUCTION

WHILE structural geology textbooks make extensive use of strain diagrams to illustrate the interrelation between, and to classify, types of finite strain ellipsoids, equivalent diagrammatic representation of stress states, however, is rarely used. Instead, most authors content themselves by providing inventories of the possible stress states accompanied by their definitions. Furthermore, although numerous finite strain diagrams have been proposed (see for example Ramsay 1967, pp. 134–139), few such diagrams exist for stress.

The choice of suitable stress diagrams should be guided by the following considerations. Firstly, it seems logical to choose a diagram which has parallel properties to widely-used finite strain diagrams. This should lead to easier understanding and wider application. Secondly, the design of the diagram should be biased by geological considerations so that the components of the (palaeo)-stress tensor that can be estimated geologically appear in a key position.

In this note two stress diagrams, one of which is proposed for the first time, will be examined. Both are the counterparts of popular strain diagrams. The new diagram has the added advantage that results of some recent methods of palaeostress analysis can be plotted on it directly. These methods are briefly reviewed and their potential application to new geological situations is suggested.

THE NADAI STRESS DIAGRAM

This diagram (Nadai 1963, p.72) represents stress states in terms of the principal deviatoric stresses σ_1', σ_2' and σ_3' where $\sigma_1' = \sigma_1 - \bar{\sigma}$, $\sigma_2' = \sigma_2 - \bar{\sigma}$, $\sigma_3' = \sigma_3 - \bar{\sigma}$ and σ_1, σ_2, σ_3, are the principal stresses and $\bar{\sigma}$ is the mean stress or hydrostatic stress component equal to $(\sigma_1+\sigma_2+\sigma_3)/3$.

The principal deviatoric stresses can be plotted on a graph with triangular coordinates (Fig. 1) because of their property that $\sigma_1' + \sigma_2' + \sigma_3' = 0$. The position of a plotted stress state is independent of its hydrostatic component. Stress states which fall on the same straight line through the origin share the same value of parameter μ

$$\mu = \frac{2\sigma_1 - \sigma_1 - \sigma_3}{\sigma_1 - \sigma_3} = \frac{2(\sigma_1 - \sigma_3) - (1)}{\sigma_1 - \sigma_3}.$$

This parameter was used by Lode for stresses applied in deformation experiments with metals to express the

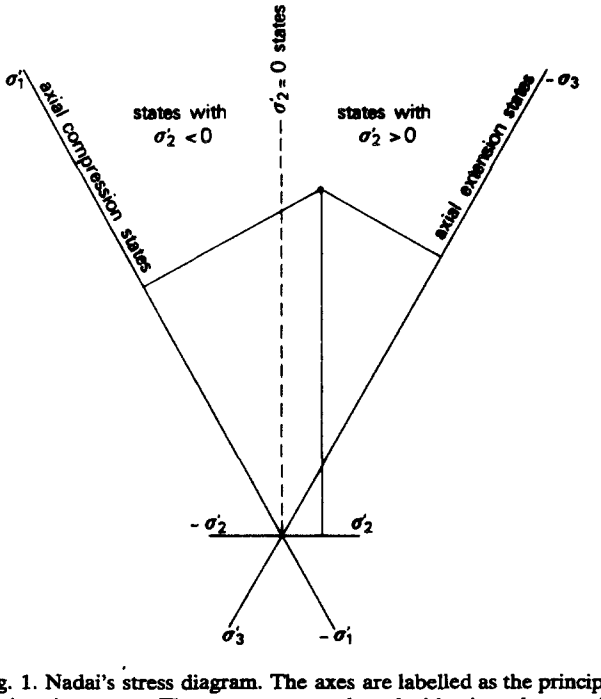

Fig. 1. Nadai's stress diagram. The axes are labelled as the principal deviatoric stresses. These stresses are plotted with triangular coordinates which is facilitated by the fact that they add up to a constant sum i.e. $\sigma_1' + \sigma_2' + \sigma_3' = 0$. Axial stress states lie along the σ_1' and σ_3' axes.

*Present address: Instituut voor Aardwetenschappen, Budapestlaan 4, 3508 TA Utrecht, The Netherlands.

position of the intermediate principal stress (σ_2) with respect to σ_1 and σ_3 (see Nadai 1931, p.77). A disadvantage of μ is that it is difficult to read off the diagram because radial lines on the diagram drawn at regular intervals of μ do not enclose equal angles.

An advantage of Nadai's diagram is, however, that the magnitude of the second deviatoric stress invariant J_2, a quantity fundamental to the theory of plasticity, is directly proportional to the distance of the plotted stress state from the origin. The diagram illustrates in direct fashion the stress required for plastic yielding of the material according to Von Mises yield criterion which predicts that yielding will occur when J_2 exceeds a certain value. The critical stress states for yielding therefore lie on a circle centred on the origin of the diagram.

The corresponding diagram for finite strain, also proposed by Nadai, was brought to the attention of structural geologists by Hossack (1968). The layout of the diagram is identical but with axes labelled with ε_1, ε_2, and ε_3 (the principal natural strains). For the simplest possible deformation involving a constant stress and coaxial strain history in a linear isotropic material, μ for the stress state will have the same value as the corresponding parameter for the finite strain v. No such correspondence will exist between the strain and stress states for more complicated deformation histories.

THE NEW STRESS DIAGRAM

The proposed diagram (Fig. 2) records the relationship between the principal stress differences by using d_1 ($= \sigma_2 - \sigma_3$) as ordinate axis and d_2 ($= \sigma_1 - \sigma_2$) as the abscissa axis. Because d_1 and d_2 are independent of the absolute magnitude of the principal stresses, the diagram cannot represent the hydrostatic component of the stress tensor the values d_1 and d_2 being closely related to the principal deviatoric stresses.

$$\sigma_1' = \tfrac{1}{3}(d_1 + 2d_2)\ \sigma_2' = \tfrac{1}{3}(d_1 - d_2)\ \sigma_3' = -\tfrac{1}{3}(2d_1 + d_2). \quad (2)$$

The quantity d_3, defined as $\sigma_1 - \sigma_3$, corresponds to what is often called the differential stress. As can be seen in Fig. 2 lines of constant d_3 have a slope of -1 and have the equation $d_1 = -d_2 + d_3$.

A hydrostatic state of stress ($\sigma_1 = \sigma_2 = \sigma_3$) plots at the origin whilst axial stress states (states with two equal principal stresses) fall along the coordinate axes of the diagram: axial extension states ($\sigma_1 = \sigma_2 > \sigma_3$, $\sigma_1' = \sigma_2' = -\frac{1}{2}\sigma_3'$) fall along the ordinate axis and axial compression states ($\sigma_1 > \sigma_2 = \sigma_3$, $\sigma_1 = -2\sigma_2 = -2\sigma_3'$) give points lying along the abscissa. As can be seen from equation (2) above, the stresses where $\sigma_2' = 0$ (plane deviatoric stress states) occur along the $d_1 = d_2$ line on the diagram.

The last three families of stress states are represented by straight lines through the origin. As will appear from later discussion, it is convenient to classify stress states into families each defining straight lines on the graph. Such lines which go through the origin define families of stress states which have the same R value, the latter defined as the gradient of the line, i.e. $R = d_1/d_2$

Other stress states

Table 1 summarises the restrictions placed on the values of the principal stresses by the definitions of some well-known stress states. These are the definitions used by Nye (1964) and Means (1976). Some stress states are defined in such a way that their plotted positions on the stress diagram occupy areas, whereas others are restricted to lines and some occupy single points. This information is summarized in Table 1 which also shows

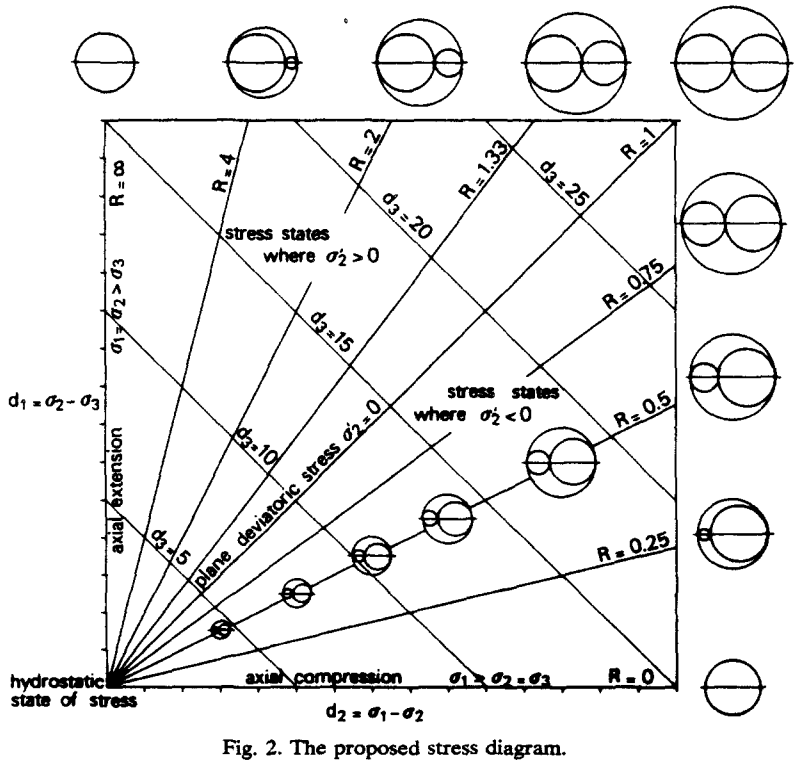

Fig. 2. The proposed stress diagram.

Table 1. Restrictions on the principal stresses

Principal Stresses			Position on diagram	Equation
α_1	α_2	α_3		
Triaxial stress states	−	−	−	Occupy *areas* on the stress diagram Stress state fields	
	+	−	−		
	+	+	−		
(no zero stresses)	+	+	+		
Biaxial stress states (plane stress) (1 zero stress)	0	−	−	Occupy *lines* on the stress diagram Stress state families	$d_1 = -2d_2 - 3\bar{\sigma}$
	+	0	−		$d_1 = d_2 - 3\bar{\sigma}$
	+	+	0		$d_1 = -\frac{1}{2}d_2 + \frac{3}{2}\bar{\sigma}$
Uniaxial stress states (2 zero stresses)	0	0	−	Uniaxial tension Occupy *points* on the diagram	$d_1 = -3\bar{\sigma}$ $d_2 = 0$
	+	0	0	Uniaxial compression	$d_1 = 0$ $d_2 = 3\bar{\sigma}$
State of No stress (3 zero stresses)	0	0	0		$d_1 = 0$ $d_2 = 0$ when $\bar{\sigma} = 0$

the equations describing the position on the plot of such lines and points. It should be noted that these equations involve the hydrostatic stress component, $\bar{\sigma}$, implying that these stress states can only be plotted on stress plots where $\bar{\sigma}$ is specified. Three examples of stress plots with specified values of $\bar{\sigma}$ are shown in Fig. 3. Particularly interesting is the position of plane stress states on these diagrams. The displacement of the $\sigma_2 = 0$ line with change in the hydrostatic component is brought out by the 3 diagrams in Fig. 3. It can be seen that from Fig. 3 and the equation for $\sigma_2 = 0$ states ($d_1 = d_2 - 3\bar{\sigma}$) that the plane stress state of this type corresponds to $R = 1$ states only in the absence of a hydrostatic component ($\bar{\sigma} = 0$). As has been pointed out by Ramsay & Wood (1973), an analogous situation exists for finite strain ellipsoids, namely that plane strain corresponds to $K = 1$ ellipsoids only in the case of no volume change, i.e. when $\bar{\varepsilon} = \frac{1}{3}\log_e(1 + \Delta) = 0$. K is a parameter for the finite strain ellipsoid defined by Flinn (1964) and directly comparable to the R value for the stress [$K = (\varepsilon_1 - \varepsilon_2)/(\varepsilon_2 - \varepsilon_3)$].

Superimposition of stress states

As is illustrated above, the diagram has parallel properties to the log Flinn diagram for finite strain. Another such property, discussed by Flinn (1979, p.296 and Fig. 2a) is that the tensor which is the product of coaxial superposition of the two tensors simplifies to a vector addition; the total tensor being the resultant of two vectors defined by joining the points representing the stress states to the origin.

SIGNIFICANCE OF THE PARAMETER *R*

As R is the ratio of the principal stress differences it is also the ratio of the principal shearing stresses (τ_{23}/τ_{12}). In Mohr's representation of the stress, R defines the shape of the arbelos (figure bounded by the circles representing the stresses in the principal planes) as opposed to its size or position on the Mohr diagram.

The ratio R, like Lode's μ, fulfills the purpose of fixing the position of σ_2 with respect to σ_1 and σ_3. These parameters are related:

$$\left[\mu = \frac{d_1 - d_2}{d_1 + d_2} = \frac{R - 1}{R + 1} \text{ and } R = \frac{1 + \mu}{1 - \mu}\right]$$

For the strain histories described above where μ (stress state) = υ (finite strain), then we find R is equal to Flinn's K.

In fact Flinn's diagram for finite strain is a companion diagram to the new stress diagram proposed here and these two diagrams have the same mutual relationship as the Nadai stress and Nadai strain diagrams.

A further property of the ratio R concerns the orientation of resolved shear stress on a plane with a particular orientation with respect to the principal axes of stress. Bott (1959, equation 7) has shown that the direction of this shear stress is determined by the ratio of the differences of the principal stresses, which we have already termed R. This property of R is utilized by the methods of stress determination described below.

THE CALCULATION OF *R* FOR GEOLOGICAL STRESSES

The method of Carey (*Carey* 1976, *Carey & Brunier* 1974, *Carey* 1979)

This determines numerically the direction of the principal stresses and a parameter simply related to R from data consisting of orientations of fault planes together with associated slickensides. The method assumes a homogeneous stress field existed within the domain from which the data was collected, and also that the slickensides all formed under influence of that same stress field. The method permits the faults themselves to

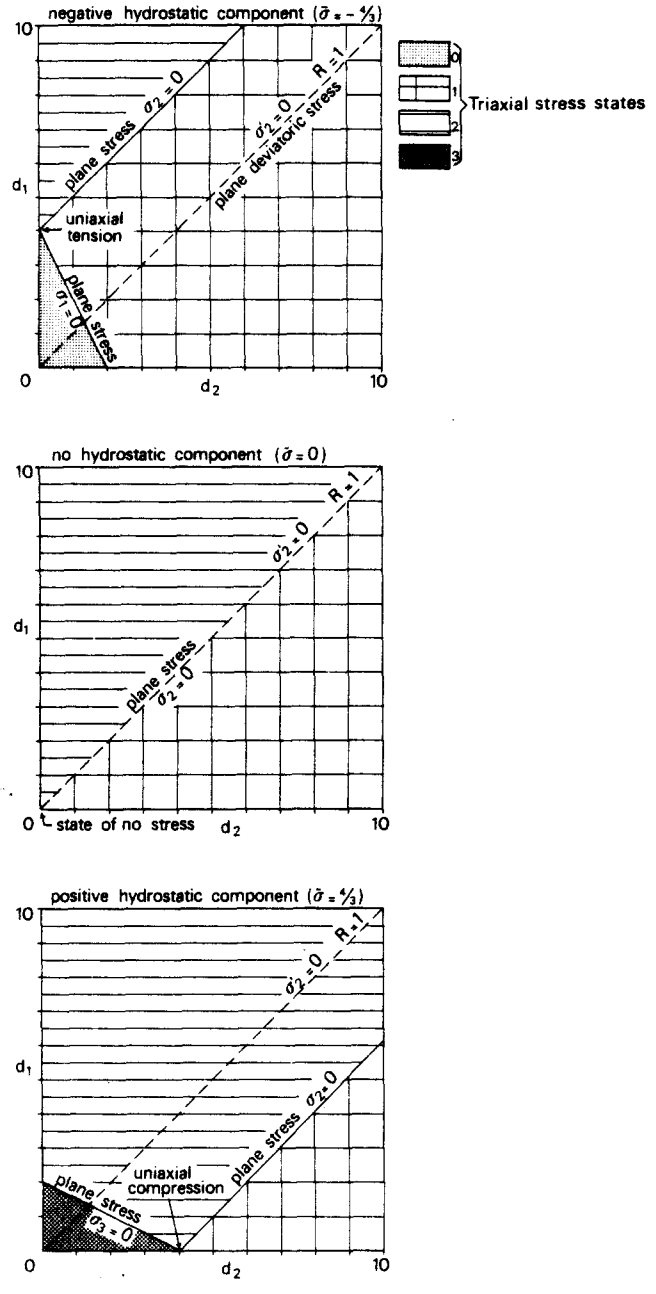

Fig. 3. Three examples of the stress plot drawn for specific values of the hydrostatic component or mean stress ($\bar{\sigma}$), to illustrate how the position of many stress states on the plot depend on $\bar{\sigma}$. The upper diagram corresponds to a negative (tensional) hydrostatic component; those below represent no- and positive hydrostatic components respectively. The different types of shading are used to distinguish different types of the triaxial stress states referred to in the key and Table 1.

have an earlier origin. There are four unknowns in the calculation and a minimum of four fault plane/slickensides combinations are needed as data.

This method of stress determination has also found application to earthquake data derived from the quadrantal pattern of compressional and dilational *P* waves.

The method of Angelier (1975, 1979)

This graphical method uses the same data as Carey's method but in addition the sense of movement has to be inferred from the character of the slickensides or from similar evidence. With respect to the orientation data from each movement plane it is possible to delimit the maximum range of possible orientations of the σ_1, and σ_3 axes. Combining data with the help of the stereographic projection leads to a reduction of the size of the orientation fields containing σ_1 and σ_3. Angelier & Mechler (1977) claim that the shapes of the fields containing possible σ_1 and σ_3 directions are an indication of $\phi = (\sigma_1 - \sigma_2)/(\sigma_1 - \sigma_3)$. R can be easily calculated from ϕ:

$$\left[R = \frac{\phi}{1 - \phi}. \right]$$

Results of these methods

Figure 4 presents the results of the methods described above. Although the number of determinations is so far small, and come from restricted types of structural regions (high-level regimes with upright structures) a tendency for low R values is clearly shown. It may not be entirely coincidental that the bulk of finite strain determinations in similar low grade rocks show a similar predominance of low K values (Wood 1973).

Possible application of these methods to other geological situations

Several methods for palaeostress determination from sheared dykes enclosed in undeformed country rocks have been described (e.g. Berger 1971, Davidson & Park 1978). Although the assumptions made are essentially those involved in the methods summarized above, these methods allow only estimation of the orientation of the principal stresses. Carey's method which provides more complete information about the stress tensor while using the same type of data, has potential application to these problems.

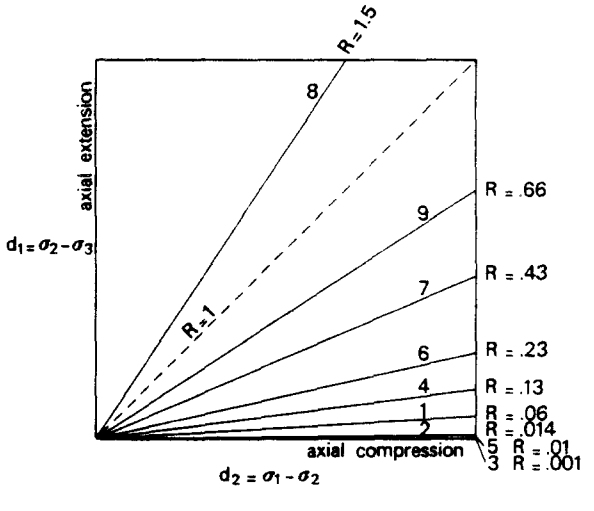

Fig. 4. Representation on the stress diagram of published palaeostress results derived from the methods described in the text. 1 - 6 are determinations carried out by Carey 1976; 1 and 2—Morvan, S. of Paris Basin, U. Jurassic; 3—near Mollendo, S. Peru, Quaternary ignimbrites; 4 and 6—Locride, C. Greece, Tertiary and Quaternary; 5—Cephalonia, W. Greece, Tertiary and Quaternary. Determinations 7 - 9 are from sites in Crete (Angelier 1975). A dominance of low R values is present in these results.

FUTURE USE OF THE DIAGRAM

The described new diagram has an obvious potential didactic use for displaying the possible variation in the deviatoric component of the stress tensor and to summarize the essential distinctions between particular stress states which in the literature have acquired special names.

A second application proposed here for the stress plot is as a means of representation of the results of stress analyses. The extent of the role to be played by the plot in this respect will depend on the completeness of results of such analyses. The methods outlined above when applied allow the non-hydrostatic part of the stress state to be restricted to a particular type or family characterized by its R value but a complete determination of the stress deviator will require supplementary information. For example, the magnitude of d_3 (the differential stress) which can be sometimes estimated on the basis of observations on the nature of faulting (Sibson 1974) or on features of a tectonite's microstructure (White 1975) would also serve to restrict the stress deviator to a linear zone on the plot, the width of which would depend on the degree of confidence placed on the estimate. In favourable circumstances it may be possible by the use of a combination of methods (for example those that yield estimates of R together with those that estimate d_3) to pin point more closely the deviatoric part of the palaeostress tensor by the intersection of the respective lines on the stress plot.

REFERENCES

Angelier, J. 1975. Sur un apport de l'informatique à l'analyse structurale; exemple de la tectonique cassante. *Rev. géogr. phys. géol. dyn.* **17,** 137–146.

Angelier, J. 1979. Determination of the mean directions of stresses from a given fault population. *Tectonophysics* **56,** T17–T26.

Angelier, J. & Mechler, P. 1977. Sur une méthode graphique de recherche des contraintes principales également utilisable en tectonique et en séismologie: La méthode des dièdres droits. *Bull. soc. géol. Fr.* **19,** 1309–1318.

Berger, A.R. 1971. Dynamic analysis using dykes with oblique internal foliations. *Bull. geol. Soc. Am.* **82,** 781–786.

Bott, M.H.P. 1959. The mechanics of oblique slip faulting. *Geol. Mag.* **93,** 109–117.

Carey, E. 1976. Analyse numérique d'un modèle mécanique elémentaire appliqué à l'étude d'une population de failles: calcul d'un tenseur moyen des contraintes à partir des stries de glissement. Thesis, Université de Paris-Sud.

Carey, E. 1979. Recherche des directions principales de constraintes associées au jeu d'une population de failles. *Rev. géogr. phys. géol. dyn.* **21,** 57–66.

Carey, E. & Brunier, B. 1974. Analyse théorique et numérique d'un modèle mécanique élémentaire appliqué à l'étude d'une population de failles. *C.R. Nebd. Séanc. Acad. Sci. Paris, série D,* **279,** 891–894.

Davidson, L.M. & Park, R.G. 1978. Late Nagssugtoquidian stress orientation derived from deformed granodiorite dykes north of Holsteinberg, West Greenland. *J. geol. Soc. Lond.* **135,** 283–290.

Flinn, D. 1964. Deformation in metamorphism. In: *Controls of Metamorphism* (edited by Pitcher, W.S. & Flinn, G.W.) Oliver & Boyd, Edinburgh, 46–72.

Flinn, D. 1978. Construction and computation of three-dimensional progressive deformations. *J. geol. Soc. Lond.* **135,** 291–305.

Hossack, J.R. 1968. Pebble deformation and thrusting in the Bygdin area (southern Norway). *Tectonophysics* **5,** 315–339.

Means, W.D. 1976. *Stress and Strain.* Springer, Berlin.

Nadai, A. 1931. *Plasticity.* McGraw-Hill, New York.

Nadai, A. 1963. *Theory of Flow and Fracture of Solids,* Vol. II, McGraw-Hill, New York.

Nye, J.F. 1964. *Physical Properties of Crystals.* Oxford University Press, London.

Ramsay, J.G. 1967. *Folding and Fracturing of Rocks.* McGraw-Hill, New York.

Ramsay, J.G. & Wood, D.S. 1973. The geometric effects of volume change during deformation processes. *Tectonophysics* **16,** 263–277

Sibson, R.H. 1974. Frictional constraints on thrust, wrench and normal faults. *Nature, Lond.* **249,** 542–544.

White, S. 1975. Estimation of strain rates from microstructures. *J. geol. Soc. Lond.* **131,** 577–583.

Wood, D.S. 1973. Patterns and magnitudes of natural strain in rocks. *Phil. Trans. R. Soc. Lond.* **A274,** 373–382.